Electronic Supplementary Information: Anharmonicities and coherent vibrational dynamics of phosphate ions in bulk H_2O

Rene Costard,*[a] Tobias Tyborski,[a] and Benjamin P. Fingerhut*[a]

Content:

[a] *Max-Born-Institut für Nichtlineare Optik und Kurzzeitspektroskopie, Max-Born-Str. 2A, D-12489 Berlin, Germany. E-mail: costard@mbi-berlin.de, fingerhut@mbi-berlin.de*

1 $H_2PO_4^- \times xH_2O$ cluster geometries

Fig. S1 shows the geometries of $H_2PO_4^- \times xH_2O$ clusters for (a) x=7 without symmetry restriction and (b) x=5 for C_2 symmetry.

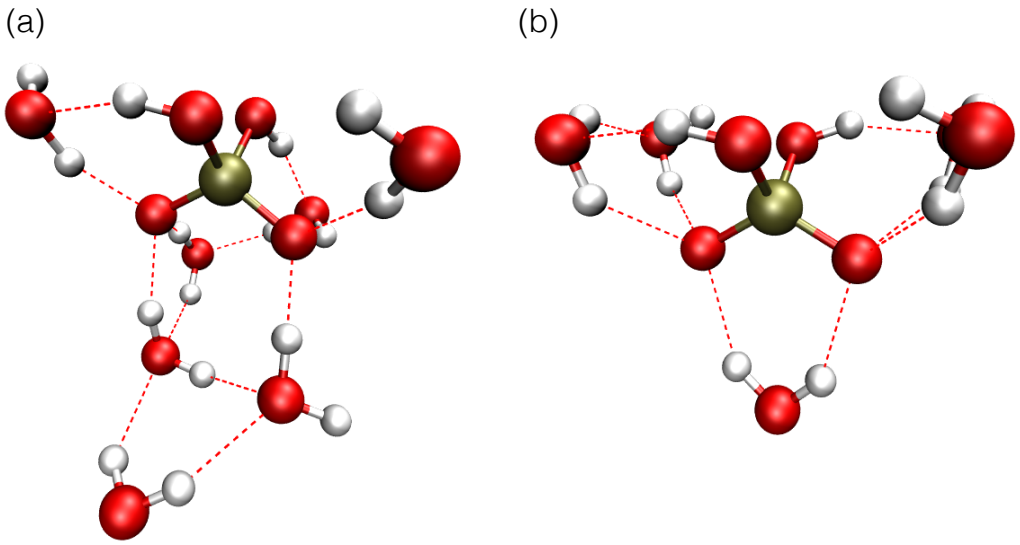

Fig. S 1 Structures of $H_2PO_4^- \times xH_2O$, $x = 5, 7$ water clusters: (a) $x = 7$, C_1 symmetry; (b) $x = 5$, C_2 symmetry .

2 Pump-probe data of ν_{AS}(P-(OH)$_2$)

In order to extract the vibrational lifetime, we performed pump-probe experiments on ν_{AS}(P-(OH)$_2$) using pulses with a bandwidth of 160 cm^{-1} (FWHM) centered at 960 cm^{-1} (cf. Fig. S2). Transient spectra at early delay times consist of reduced absorption signal centered around 955 cm^{-1} due to ground state bleach and stimulated emission after excitation of the v=1 state, whereas the red-shifted enhanced absorption is caused by the excited state absorption. Vibrational lifetimes are extracted from the decay of the excited state absorption at 928 cm^{-1} (Fig. S2b) that shows a characteristic time constant of 450 fs.

Note that transient spectra at a delay time of 2 ps show a residual absorbance change consisting of an enhanced absorption in the red and a reduced absorption in the blue part of the spectrum. Such signals remain constant on a picosecond timescale and are a hallmark of weakened phosphate-water hydrogen bonds due to the dissipation of excess energy into the water solvent. Such a response is similar to the one of the PO_2^- stretching vibrations[1], however, ν_{AS}(P-(OH)$_2$) shifts to the opposite direction, i.e., to the red. This result is in agreement with the cluster analysis that suggests a blue-shift of ν_{AS}(P-(OH)$_2$) upon solvation whereas the PO_2^- stretching vibration shift to the red.

3 Simulation details of nonlinear response function

3.1 Simulation of 2D spectra

Linear absorption and 2D IR signals are simulated in the sum-over-states approach with the response function evaluated by the cumulant expansion of Gaussian fluctuations[2–4]. We employ the Doorway-Window

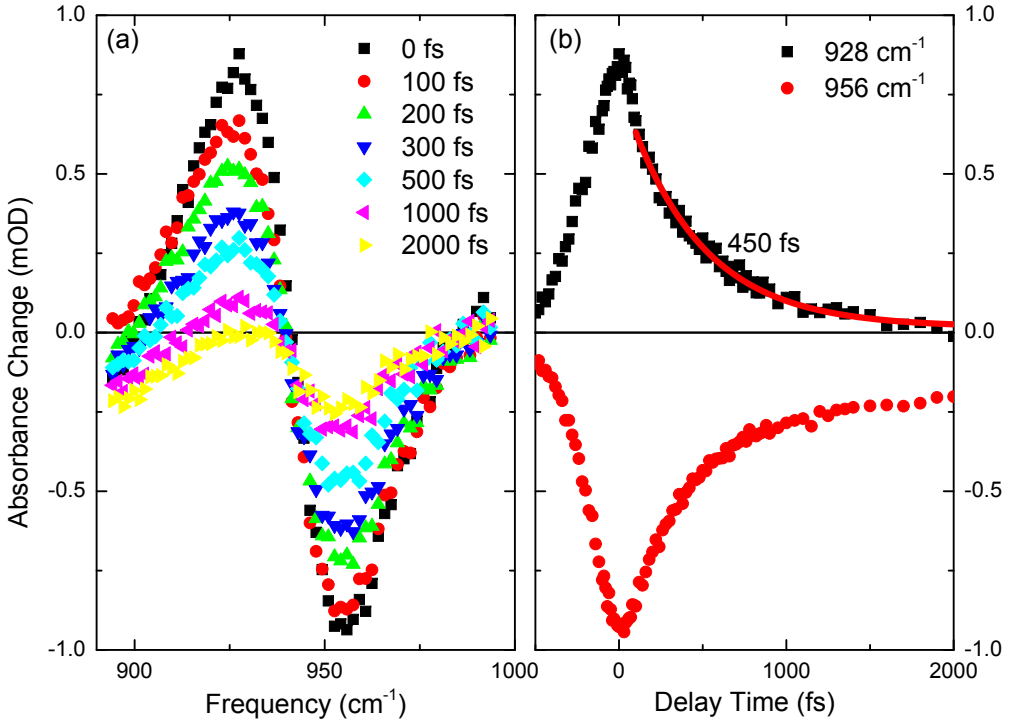

Fig. S 2 Pump-probe data of the ν_{AS}(P-$(OH)_2$) stretching mode measured with infrared pulses centered at 960 cm^{-1}: (a) Transient spectra between 0 fs and 2ps; (b) Decays of the signals at fixed probe frequencies.

factorization[4,5] of the third order response function

$$\hat{R}(t_3,t_2,t_1) = R^{(c)}(t_3,t_2,t_1) + \sum_{\mu,\nu} W_\mu(t_3) G_{\mu\nu}(t_2) D_\nu(t_1) + W_0(t_3) D_0(t_1) \tag{1}$$

where $R^{(c)}$ denotes the coherent contribution to the response function, $G_{\mu\nu}$ is the Green's function describing exciton hopping and W_μ and D_ν, as well as W_0 and D_0, represent Doorway- and Window-wavepackets, respectively. $R^{(c)}(t_3,t_2,t_1)$ is given by

$$R^{(c)}(t_3,t_2,t_1) = R(t_3,t_2,t_1) - R(t_3,\infty,t_1). \tag{2}$$

Invoking the RWA, the coherent contributions for the rephasing photon echo signal ($k_I = -k_1 + k_2 + k_3$) are given as

$$R^{(c)}_{\mathbf{k_I}}(t_3,t_2,t_1) = R_I(t_3,t_2,t_1) + R_{II}(t_3,t_2,t_1) + R_{III}(t_3,t_2,t_1) \tag{3}$$

$$\begin{aligned} R_I(t_3,t_2,t_1) = -i \sum_{\mu\nu} d_\mu d_\mu d_\nu d_\nu \exp(-f^{(1)}_{\mu\nu}(0,t_2+t_1,t_3+t_2+t_1,t_1)) \times \\ \exp(-i\varepsilon_\mu(t_3+t_2) + i\varepsilon_\nu(t_2+t_1)) \end{aligned} \tag{4}$$

$$\begin{aligned} R_{II}(t_3,t_2,t_1) = -i \sum_{\mu\nu} d_\mu d_\mu d_\nu d_\nu \exp(-f^{(1)}_{\mu\nu}(0,t_1,t_3+t_2+t_1,t_2+t_1)) \times \\ \exp(-i\varepsilon_\mu t_3 + i\varepsilon_\nu t_1) \end{aligned} \tag{5}$$

$$R_{III}(t_3,t_2,t_1) = -i\{\sum_{\mu\nu\overline{\alpha}} d_{\mu\overline{\alpha}}d_{\nu\overline{\alpha}}d_\nu d_\mu \exp(-f^{(2)}_{\mu\nu,\overline{\alpha}}(t_1,t_2+t_1,t_3+t_2+t_1,0))\times \\ \exp(-i\varepsilon_\mu(t_3+t_2+t_1)+i\varepsilon_{\overline{\alpha}}t_3+i\varepsilon_\nu t_2)\}^* \tag{6}$$

where μ,ν and $\overline{\alpha}$ denote single and bi-exciton states, respectively, with state energies ε_i, dipole moments d_i and the auxiliary functions $f^{(1)}_{\mu\nu}$ and $f^{(2)}_{\mu\nu,\overline{\alpha}}$. The coherent contributions of the non-rephasing signal ($k_{II} = +k_1-k_2+k_3$) read

$$R^{(c)}_{\mathbf{k_{II}}}(t_3,t_2,t_1) = R_{IV}(t_3,t_2,t_1)+R_V(t_3,t_2,t_1)+R_{VI}(t_3,t_2,t_1) \tag{7}$$

$$R_{IV}(t_3,t_2,t_1) = -i\sum_{\mu\nu} d_\mu d_\mu d_\nu d_\nu \exp(-f^{(1)}_{\mu\nu}(t_1,t_2+t_1,t_3+t_2+t_1,0))\times \\ \exp(-i\varepsilon_\mu(t_3+t_2+t_1)+i\varepsilon_\nu(t_2)) \tag{8}$$

$$R_V(t_3,t_2,t_1) = -i\sum_{\mu\nu} d_\mu d_\mu d_\nu d_\nu \exp(-f^{(1)}_{\mu\nu}(t_3+t_2+t_1,t_2+t_1,t_1,0))\times \\ \exp(-i\varepsilon_\mu t_1+i\varepsilon_\nu t_3) \tag{9}$$

$$R_{VI}(t_3,t_2,t_1) = -i\{\sum_{\mu\nu\overline{\alpha}} d_{\mu\overline{\alpha}}d_{\nu\overline{\alpha}}d_\nu d_\mu \exp(-f^{(2)}_{\mu\nu,\overline{\alpha}}(t_1,t_3+t_2+t_1,t_2+t_1,0))\times \\ \exp(-i\varepsilon_\mu(t_2+t_1)+i\varepsilon_{\overline{\alpha}}t_3+i\varepsilon_\nu(t_2+t_3)\}^* \tag{10}$$

with $f^{(1)}_{\mu\nu}$ and $f^{(2)}_{\mu\nu,\overline{\alpha}}$ in eqs. 4-10 given by

$$f^{(1)}_{\mu\nu} = g_{\mu\mu}(\tau_2-\tau_1)-g_{\mu\nu}(\tau_3-\tau_1)+g_{\mu\nu}(\tau_4-\tau_1) \\ +g_{\mu\nu}(\tau_3-\tau_2)-g_{\mu\nu}(\tau_4-\tau_2)+g_{\mu\mu}(\tau_4-\tau_3) \tag{11}$$

and

$$f^{(2)}_{\mu\nu,\overline{\alpha}} = g_{\mu\mu}(\tau_2-\tau_1)-g_{\mu\overline{\alpha}}(\tau_2-\tau_1)+g_{\mu\overline{\alpha}}(\tau_3-\tau_1)-g_{\mu\nu}(\tau_3-\tau_1)+g_{\mu\nu}(\tau_4-\tau_1) \\ -g_{\mu\overline{\alpha}}(\tau_3-\tau_2)+g_{\mu\nu}(\tau_3-\tau_2)-g_{\mu\nu}(\tau_4-\tau_2)+g_{\overline{\alpha}\overline{\alpha}}(\tau_3-\tau_2)-g_{\overline{\alpha}\nu}(\tau_3-\tau_2) \\ +g_{\overline{\alpha}\nu}(\tau_4-\tau_2)-g_{\overline{\alpha}\nu}(\tau_4-\tau_3)+g_{\mu\nu}(\tau_4-\tau_3). \tag{12}$$

Here $g(\tau)$ denotes the lineshape functions of single (μ,ν) and bi-exciton $(\overline{\alpha})$ states.

The cumulant expansion of Gaussian fluctuations formulation of the response function holds for purely diagonal frequency fluctuations with arbitrary timescales; Population relaxation can be incorporated perturbatively in the off-diagonal fluctuations by employing the Doorway-Window factorization with the Doorway-wavepacket D describing the preparation process and the Window-wavepacket W describing detection:

$$\sum_{\mu\nu} W_\mu(t_3)G_{\mu\nu}(t_2)D_\nu(t_1) = -i\sum_{\mu\nu} d^2_\nu \exp(i\varepsilon_\nu t_1-g^*_{\nu\nu})G_{\mu\nu}(t_2)\times \\ [d^2_\mu \exp(-i\varepsilon_\mu t_3-g^*_{\mu\mu}+2i\lambda_{\mu\mu}t_3) \\ -\sum_{\overline{\nu}} d^2_{\mu\overline{\nu}}\exp(-i(\varepsilon_{\overline{\nu}}-\varepsilon_\mu)t_3-g_{\mu\mu}(t_3)-g_{\overline{\nu}\overline{\nu}}(t_3)+2g_{\mu\overline{\nu}}(t_3)+2i(\lambda_{\mu\overline{\nu}}-\lambda_{\nu\nu})t_3)] \tag{13}$$

where the exciton reorganization energy is given by

$$\lambda_{\mu\nu} = -\lim_{\tau\to\infty} Im\left[\frac{dg_{\mu\nu(\tau)}}{d\tau}\right]. \tag{14}$$

Incoherent transport within the secular approximation is incorporated phenomenologically by the Green's function of the generalized master equation for exciton-hopping $G_{\mu\nu}(t_2)$ and accounts for the experimentally observed lifetime broadening ($1/k_{\mu 0} = 300$ fs), while inter-mode transport ($k_{\mu\nu}$) is neglected. The coherent part $R^{(c)}(t_3,t_2,t_1)$ of the response function is responsible for the observed quantum beats (cf. Fig. 5-6; Fig. S3-S5) in 2D and pump-probe signals.

The long time response

$$R(t_3,\infty,t_1) = \sum_{\mu} W_\mu(t_3)D_\mu(t_1) + W_0(t_3)D_0(t_1) \tag{15}$$

with

$$\begin{aligned}\sum_{mu} W_\mu(t_3)D_\mu(t_1) = -i\sum_{\mu} d_\mu^2 \exp(i\varepsilon_\mu t_1 - g^*_{\mu\mu}(t_1))\{d^2\exp(-i\varepsilon_\mu t_3 - g^*_{\mu\mu}(t_3) + 2i\lambda_{\mu\mu}t_3) \\ -\sum_{\overline{\nu}} d^2_{\mu,\overline{\nu}}\exp(-i(\varepsilon_{\overline{\nu}} - \varepsilon_\mu)t_3 - g_{\mu\mu}(t_3) - g_{\overline{\nu}\overline{\nu}}(t_3) + 2g_{\mu\overline{\nu}}(t_3) + 2i(\lambda_{\mu\overline{\nu}} - \lambda_{\mu\mu})t_3)\}\end{aligned} \tag{16}$$

and

$$W_0(t_3)D_0(t_1) = -i\sum_{\mu\nu} d_\nu^2 d_\mu^2 \exp(i\varepsilon_\nu t_1 - g^*_{\nu\nu}(t_1))\exp(-i\varepsilon_\mu t_3 - g_{\mu\mu}(t_3)) \tag{17}$$

has minor contributions for the evaluated delay times < 1 ps. The delay time T used in the main paper corresponds to t_2. 2D absorptive signals are obtained by a 2D Fourier transform of the time-domain response function $\hat{R}(t_3,t_2,t_1)$ followed by summation of the real parts of the rephasing and non-rephasing signals[6,7].

Lineshape function g(t):

The lineshape function of the over damped Brownian oscillator (OBO) model in the high temperature limit is given by[3]

$$\begin{aligned}g(t) = \frac{2\lambda k_B T}{\hbar\Lambda^2}\left[exp(-\Lambda t) + \Lambda t - 1\right] \\ -i(\lambda/\Lambda)\left[exp(-\Lambda t) + \Lambda t - 1\right].\end{aligned} \tag{18}$$

By assuming a real valued classical frequency-frequency correlation function (main text, eq.1) the OBO model can be simplified to the stochastic Kubo model[8]. For the parametrization of eq. 18 we fit the parameters (oscillator timescale Λ, fluctuation bandwidth $\delta\nu_{hom}$) of a Kubo model with static offset $\delta\nu_{static}$ to the frequency-frequency fluctuation correlation function directly calculated from the fluctuations of instantaneous frequencies of the hybrid QM/MM trajectory (cf. Ref. 1, Λ = 50 fs). By recognizing the relation $\lambda = \delta\nu^2_{hom}/2k_BT$ the OBO model can be fully parametrized from the instantaneous frequency fluctuations of the classical trajectories. The derived (static) inhomogeous contribution is used for the generation of random single-exciton Hamiltonians centered around the single exciton transition frequency ω_i with Gaussian width $\delta\nu_{i,static}$.

3.2 Lineshape analysis of diagonal peaks

In section 2.2.1 of the main paper, we analyze the frequency fluctuations of ν_{AS}(P-(OH)$_2$) by fitting the calculated third-order nonlinear response to the experimental spectra. For the calculation we use the six Feynman diagrams that describe the rephasing (eq. 19) and non-rephasing (eq. 20) contribution to the GSB,SE and ESA[3,7]. The used response functions reads

$$R_{I,II,III}(\tau,T,t) = \left(e^{-i\omega_{01}(t-\tau)} - e^{-i((\omega_{01}-\Delta)t-\omega_{01}\tau)}\right) e^{-(\tau+t)/(2T_1)} e^{-(\tau+t)/T_2^*} \\ e^{-T/T_1} \cdot e^{-g(\tau)+g(T)-g(t)-g(\tau+T)-g(T+t)+g(\tau+T+t)} \tag{19}$$

$$R_{IV,V,VI}(\tau,T,t) = \left(e^{-i\omega_{01}(t+\tau)} - e^{-i((\omega_{01}-\Delta)t+\omega_{01}\tau)}\right) e^{-(\tau+t)/(2T_1)} e^{-(\tau+t)/T_2^*} \\ e^{-T/T_1} \cdot e^{-g(\tau)-g(T)-g(t)+g(\tau+T)+g(T+t)-g(\tau+T+t)} \tag{20}$$

and can be obtained from the formalism described in[2,3,5] and outlined above by neglecting transport contributions. Here, ω_{01} is the transition frequency corresponding to 940 cm^{-1}, Δ ist the anharmonicity (12 cm^{-1}), T_2^* is the pure dephasing time used as a fit parameter, T_1 is the vibrational lifetime (450 fs), and $g(t)$ is the line shape function of the Kubo model. Since the latter is only used to describe the minor inhomogeneous broadening, the single free parameter is the distribution of frequencies $\Delta\omega_{inh}$: $g(t) = \Delta\omega_{inh}^2 t^2/2$.

4 Coherent wave packet dynamics

4.1 Pump probe: Beating of PO_2^- modes

In the manuscript we followed the wave packet dynamics of $\nu_S(PO_2^-)$ and $\nu_{AS}(PO_2^-)$ through the relative amplitudes of 2D cross peaks. Pump-probe data as presented in ref. 1 with a better sampling of the delay times provides additional proof of the underlying dynamics. The oscillatory contribution to the signals at a frequency of 1170 cm^{-1} are shown in Fig. S3a which presents residuals of a multiexponential fit to the experimental data (cf. inset). The power spectrum of the oscillatory feature has a peak at $\approx$ 90 cm^{-1}, corresponding to the difference frequency of $\nu_S(PO_2^-)$ and $\nu_{AS}(PO_2^-)$.

4.2 Decomposition of 2D spectra into rephasing and non-rephasing components

Experimental absorptive 2D spectra are decomposed into the underlying rephasing and nonrephasing spectra in Fig. S4. All spectra were normalized to a 300 fs decay corresponding to the vibrational lifetime of $\nu_S(PO_2^-)$ and $\nu_{AS}(PO_2^-)$. The same scale was used for absorptive, rephasing and non-rephasing spectra to facilitate a direct comparison of the different signal contributions. The tilt of the cross peaks shown in the absorptive spectra (Fig. 5, main paper) can be rationalized by the time-dependent cross peak amplitude in the rephasing signal.

For T = 0 fs the tilt of SE and ESA cross peaks relative to the ν_1 axis originates from the tilting of the rephasing cross peak with respect to the ν_1 axis while the non-rephasing cross peak appears upright. For increased waiting time (T = 100 fs) the rephasing cross peak intensity is reduced leading to a reduced cross peak tilt in the absorptive 2D signal. The reversed tilt for T=200 fs arises from the interplay of signal evolution in rephasing and non-rephasing contributions: the rephasing cross peak intensity reaches its minimum while non-rephasing cross peak intensity appears practically constant. Accordingly the non-rephasing contribution with anti-diagonal tilt becomes the dominant contribution to the absorptive cross-

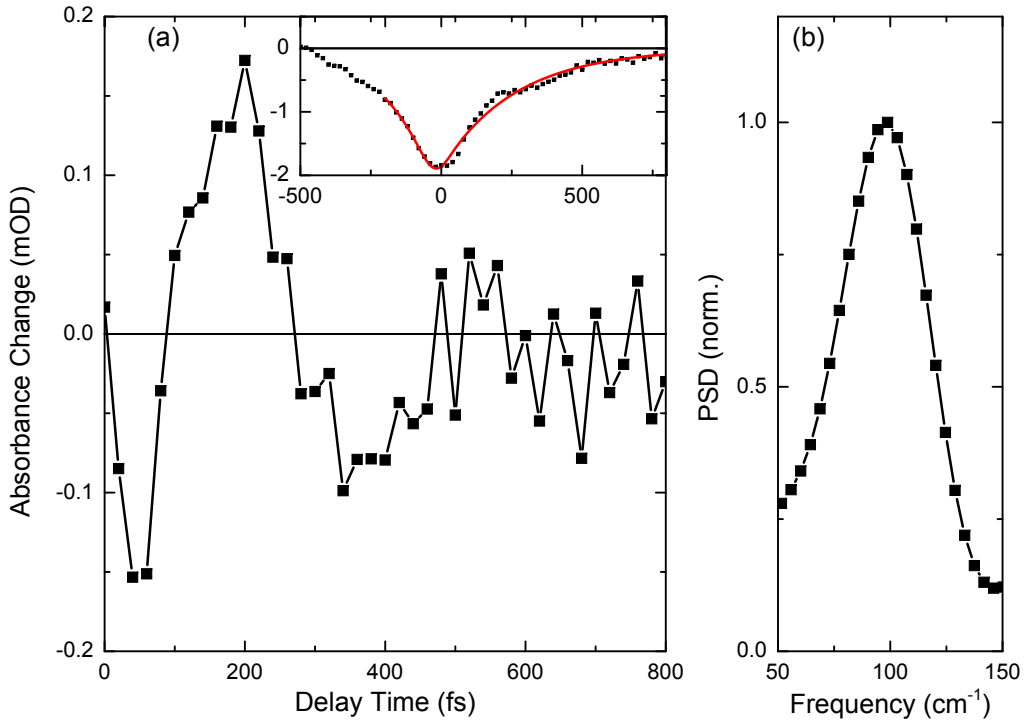

Fig. S 3 Extraction of the oscillatory part in $\nu_{AS}(PO_2^-)$. (a) Oscillatory part of the pump-probe signal measured at 1170 cm^{-1} which was extracted by subtracting a multi-exponential fit from the total pump-probe response (cf. inset, experiment: symbols, multiexponential fit: red line). (b) Normalized power spectrum of the Fourier transform of the oscillatory signal.

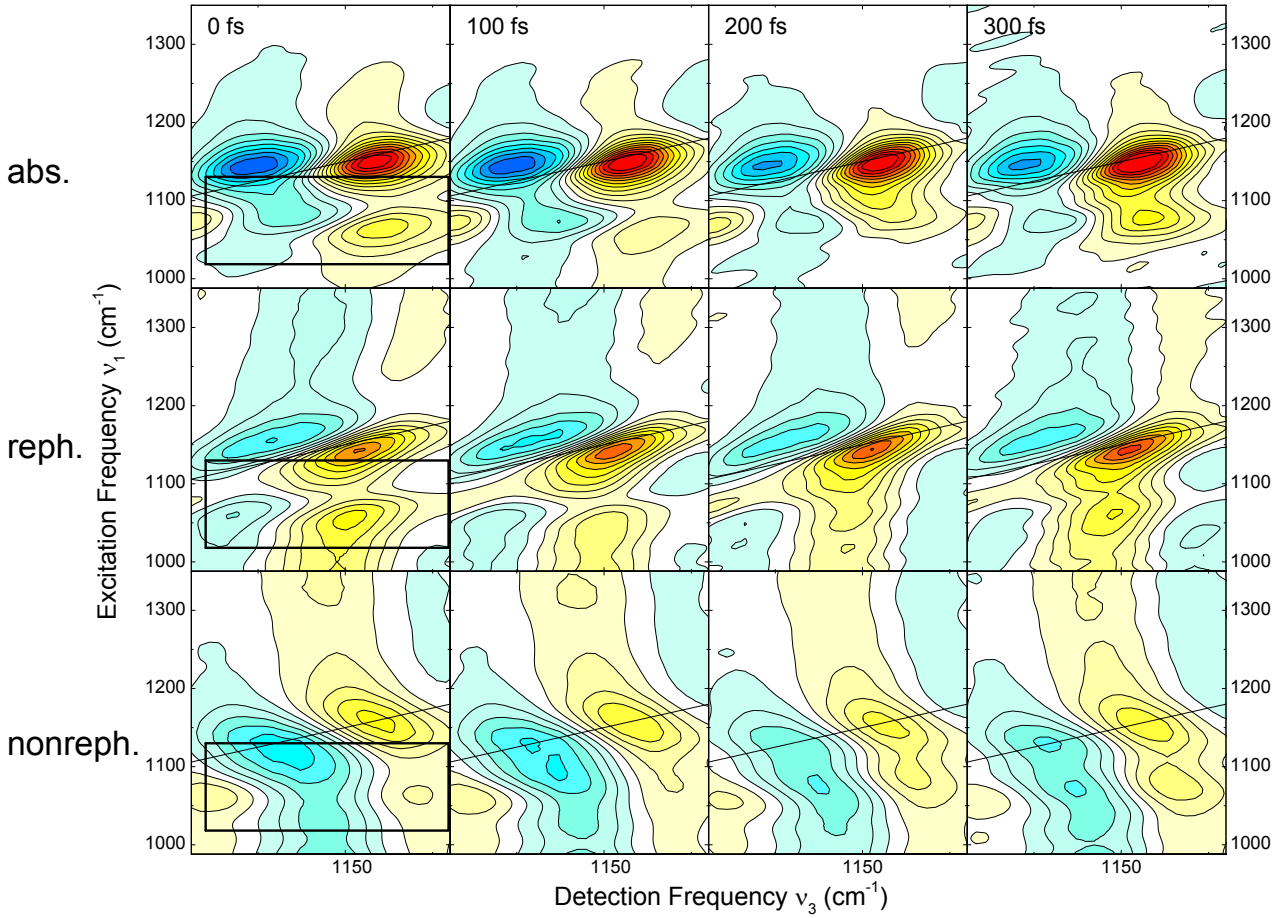

Fig. S 4 Dissection of the oscillatory part in crosspeak (ν_1, ν_3)=($\nu_S(PO_2^-)$,$\nu_{AS}(PO_2^-)$): (a) absorptive 2D signal, (b) rephasing 2D signal, (c) non-rephasing 2D signal for delay times T = 0, 100, 200, 300 fs, respectively. The signals have been normalized to a 300 fs decay imposed by the lifetime of $\nu_{AS}(PO_2^-)$ and $\nu_S(PO_2^-)$ modes. The boxes in the first panel of each row enclose the cross peaks shown in Fig. 5 of the manuscript.

peak for T=200 fs. As the rephasing cross peak intensity increases again for T=300 fs the opposite tilts of rephasing and non-rephasing cross peaks cancel and the absorptive 2D signal appears upright.

4.3 Coherent oscillations in the reduced two-state model

Fig. S5 presents 2D spectra of the reduced model which takes into account energy levels of $\nu_{AS}(PO_2^-)$ and $\nu_{AS}(PO_2^-)$ stretching modes together with the dark Fermi-resonance mode and neglects contributions of bending modes (δ_{AS}(P-(OH)$_2$), δ_S(P-(OH)$_2$)) and the ν_{AS}(P-(OH)$_2$) stretching mode. The reduced model is designed to closely resemble the experimental excitation conditions which due to the limited spectral bandwidth of pulses coherently excite $\nu_{AS}(PO_2^-)$ and $\nu_{AS}(PO_2^-)$ stretching modes only. The inlay shows coherent beating of diagonal (dashed) and off-diagonal peaks (solid) at the position of the ESA and SE contribution together with their Fourier transform. The coherent beating at different positions (diagonal and off-diagonal peaks) arise from the non-rephasing and rephasing contributions to the absorptive signals.

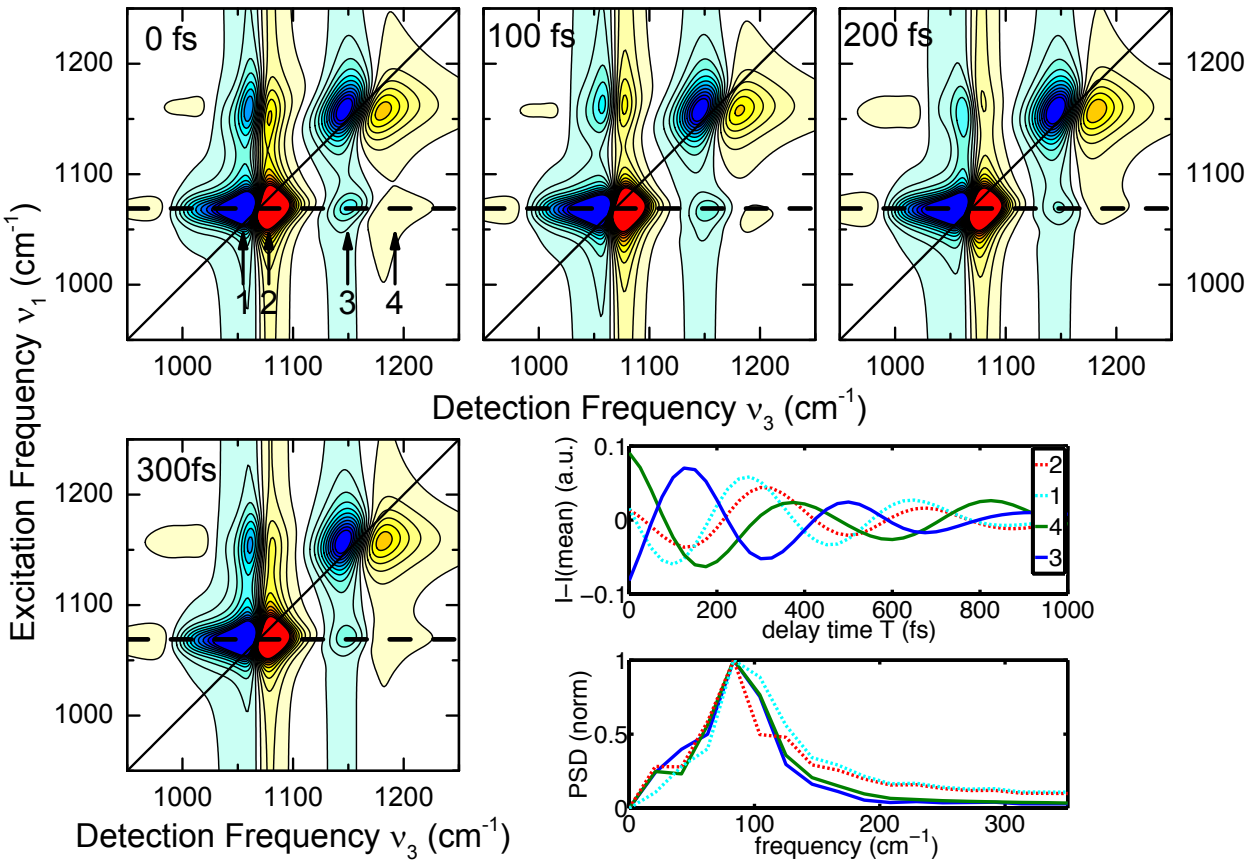

Fig. S 5 2D spectra of the reduced model consisting of $\nu_{AS}(PO_2^-)$ and $\nu_{AS}(PO_2^-)$ stretching modes together with the dark Fermi-resonance mode for waiting time $T = 0$, 100, 200, 300 fs. The inlay shows coherent beating of diagonal (dashed) and off-diagonal peaks (solid) at the position of the ESA and SE contribution together with the normalized power spectrum of the Fourier transform of the oscillatory signal.

References

1 R. Costard, T. Tyborski, B. P. Fingerhut and T. Elsaesser, *J. Chem. Phys.*, 2015, **142**, 212406.
2 T. Meier, V. Chernyak and S. Mukamel, *J. Chem. Phys.*, 1997, **107**, 8759–8780.
3 S. Mukamel, *Principles of Nonlinear Optical Spectroscopy (Oxford Series on Optical and Imaging Sciences)*, Oxford University Press, USA, 3rd edn, 1999.
4 D. Abramavicius, B. Palmieri, D. V. Voronine, F. Šanda and S. Mukamel, *Chem. Rev.*, 2009, **109**, 2350–2408.
5 W. M. Zhang, T. Meier, V. Chernyak and S. Mukamel, *J. Chem. Phys.*, 1998, **108**, 7763–7774.
6 M. Khalil, N. Demirdöven and A. Tokmakoff, *Phys. Rev. Lett.*, 2003, **90**, 047401.
7 P. Hamm and M. Zanni, *Concepts and Methods of 2D Infrared Spectroscopy*, Cambridge University Press, 1st edn, 2011.
8 E. T. J. Nibbering, K. Duppen and D. A. Wiersma, *J. Photochem. Photobiol. A: Chemistry*, 1992, **62**, 347 – 370.

Table. S 1 Calculated IR frequencies and intensities of $H_2PO_4^-$ (in cm^{-1}): top - mean instantaneous frequencies from hybrid QM/MM trajectory; bottom - $H_2PO_4^-$ × 5 H_2O on *VSCF* / DFT(PBE0)level of theory (C_2 symmetry); Basis: 6-311++G(d,p) diagonal anharmonicity: $\Delta_{20} = 2 * \nu_{VSCF/VCI}(v{=}0{\rightarrow}1)$ - $\nu_{VSCF/VCI}(v{=}0{\rightarrow}2)$; [a] VSCF (VCI) level of theory.

Model	Mode	H.O.	Diagonal	VSCF	Δ_{20}	VCI	Δ_{20}	Int. [a.u.] [a]
$H_2PO_4^-$ *solv.* (QMMM):								
	δ_{AS}(P-$(OH)_2$)	1249.4						
	δ_S(P-$(OH)_2$)	1224.5						
	ν_{AS}(PO_2)	1158.0						
	ν_S(PO_2)	1069.0						
	ν_{AS}(P-$(OH)_2$)	923.2						
$H_2PO_4^-$ ×5H_2O:								
	ν_{AS}($(OH)_2$)	3519.8	3416.6	3358.7	115.1	3287.4	17.6	23.8
	ν_S($(OH)_2$)	3513.0	3607.0	3259.6	279.6	3201.6	309.3	966.8
	δ_{AS}(P-$(OH)_2$)	1300.3	1310.3	1292.8	2.0	1288.8	5.17	318.9
	δ_S(P-$(OH)_2$)	1227.8	1253.7	1216.0	-2.5	1201.0	22.45	53.3
	ν_{AS}(PO_2)	1165.1	1173.6	1155.4	4.0	1150.0	8.9	200.2
	ν_S(PO_2)	1065.9	1063.9	1058.7	4.8	1058.0	15.05	214.3
	ν_{AS}(P-$(OH)_2$)	887.2	894.6	894.8	2.4	897.7	27.7	387.1
	δ(O=P=O)	514.7	517.2	524.7	-2.0	525.2	0.0	89.7